J. Biochem. 2012;151(2):167–178 doi:10.1093/jb/mvr125

JB THE JOURNAL OF BIOCHEMISTRY

Structural insights into the substrate specificity of bacterial copper amine oxidase obtained by using irreversible inhibitors

Received August 22, 2011; accepted September 29, 2011; published online October 7, 2011

Takeshi Murakawa[1], Hideyuki Hayashi[1], Masayasu Taki[2], Yukio Yamamoto[2], Yoshiaki Kawano[3], Katsuyuki Tanizawa[4] and Toshihide Okajima[1,4,*]

[1]Department of Biochemistry, Osaka Medical College, Osaka 569-8686; [2]Graduate School of Human and Environmental Studies, Kyoto University, Kyoto 606-8501; [3]Institute of Physical and Chemical Research, RIKEN Harima Institute/SPring-8, Hyogo 679-5148; and [4]Institute of Scientific and Industrial Research, Osaka University, Osaka 567-0047, Japan

*Toshihide Okajima, Institute of Scientific and Industrial Research, Osaka University, Ibaraki, Osaka 567-0047, Japan.
Tel: +81-6-6879-4292, Fax: +81-6-6879-8460,
email: tokajima@sanken.osaka-u.ac.jp

Copper amine oxidases (CAOs) catalyse the oxidation of various aliphatic amines to the corresponding aldehydes, ammonia and hydrogen peroxide. Although CAOs from various organisms share a highly conserved active-site structure including a protein-derived cofactor, topa quinone (TPQ), their substrate specificities differ considerably. To obtain structural insights into the substrate specificity of a CAO from *Arthrobacter globiformis* (AGAO), we have determined the X-ray crystal structures of AGAO complexed with irreversible inhibitors that form covalent adducts with TPQ. Three hydrazine derivatives, benzylhydrazine (BHZ), 4-hydroxybenzylhydrazine (4-OH-BHZ) and phenylhydrazine (PHZ) formed predominantly a hydrazone adduct, which is structurally analogous to the substrate Schiff base of TPQ formed during the catalytic reaction. With BHZ and 4-OH-BHZ, but not with PHZ, the inhibitor aromatic ring is bound to a hydrophobic cavity near the active site in a well-defined conformation. Furthermore, the hydrogen atom on the hydrazone nitrogen is located closer to the catalytic base in the BHZ and 4-OH-BHZ adducts than in the PHZ adduct. These results correlate well with the reactivity of 2-phenylethylamine and tyramine as preferred substrates for AGAO and also explain why benzylamine is a poor substrate with markedly decreased rate constants for the steps of proton abstraction and the following hydrolysis.

Keywords: copper amine oxidase/irreversible inhibitor/substrate specificity/topa quinone/X-ray crystal structure.

Abbreviations: AGAO, BSAO, ECAO and HPAO, are copper amine oxidases from *Arthrobacter globiformis*, bovine serum, *Escherichia coli* and *Hansenula polymorpha*, respectively; BHZ, benzylhydrazine; CAO, copper amine oxidase; 2-HP, 2-hydrazinopyridine; 4-OH-BHZ, 4-hydroxybenzylhydrazine; PEA, 2-phenylethylamine; PHZ, phenylhydrazine; TPQ, topa quinone; TPQ_{psb}, product Schiff base of TPQ; TPQ_{ssb}, substrate Schiff base of TPQ; TPQ_{ox}, oxidized form of TPQ; TPQ_{red}, reduced (aminoresorcinol) form of TPQ; TPQ_{sq}, semiquinone radical form of TPQ.

Copper amine oxidases (CAOs) catalyse the oxidative deamination of various primary aliphatic amines to the corresponding aldehydes with concomitant generation of ammonia and hydrogen peroxide (*1*, *2*). All CAOs that have been structurally well characterized form homodimers with each subunit between 70 and 95-kDa in size. Each subunit contains a Cu^{2+} ion and a quinone cofactor designated topa quinone (TPQ) that is produced post-translationally from a specific tyrosine residue encoded in the polypeptide chain (*3-5*). The overall catalytic reaction of CAOs commonly proceeds through the ping–pong bi–bi mechanism and consists of reductive and oxidative half-reactions involving the $2\,e^-$-reduction of TPQ by the substrate and re-oxidation of TPQ by molecular oxygen, respectively (Scheme 1) (*6-8*). In the reductive half-reaction, the protonated substrate amine first forms a Michaelis complex with the enzyme containing the oxidized cofactor (TPQ_{ox}) and a proton derived from the substrate is presumably captured by the conserved Asp residue (catalytic base), which is initially deprotonated [We have recently obtained evidence that the C4 hydroxyl group of TPQ_{ox} (but not the conserved Asp) accepts a proton from the substrate amino group and that TPQ_{ssb} is formed without participation of the conserved Asp (Murakawa *et al.*, unpublished data)]. Nucleophilic attack of the deprotonated amino group of the substrate onto the C5 carbonyl group of TPQ_{ox} yields a carbinolamine-like intermediate of TPQ (step $A \rightarrow B$). The substrate Schiff base intermediate (TPQ_{ssb}) is then formed with the release of a water molecule (step $B \rightarrow C$). The deprotonated Asp residue abstracts the Cα proton of the substrate in a stereospecific manner (*9*), thereby forming the product Schiff base intermediate (TPQ_{psb}) with the reduction of the cofactor ring (step $C \rightarrow D$). TPQ_{psb} is hydrolysed to form the first product aldehyde and the reduced cofactor in an aminoresorcinol form (TPQ_{red}) (steps $D \rightarrow D' \rightarrow E$). Thus, the conserved Asp residue plays an indispensable role during the reductive half-reaction. In the oxidative half-reaction, TPQ_{red} is oxidized by molecular oxygen to

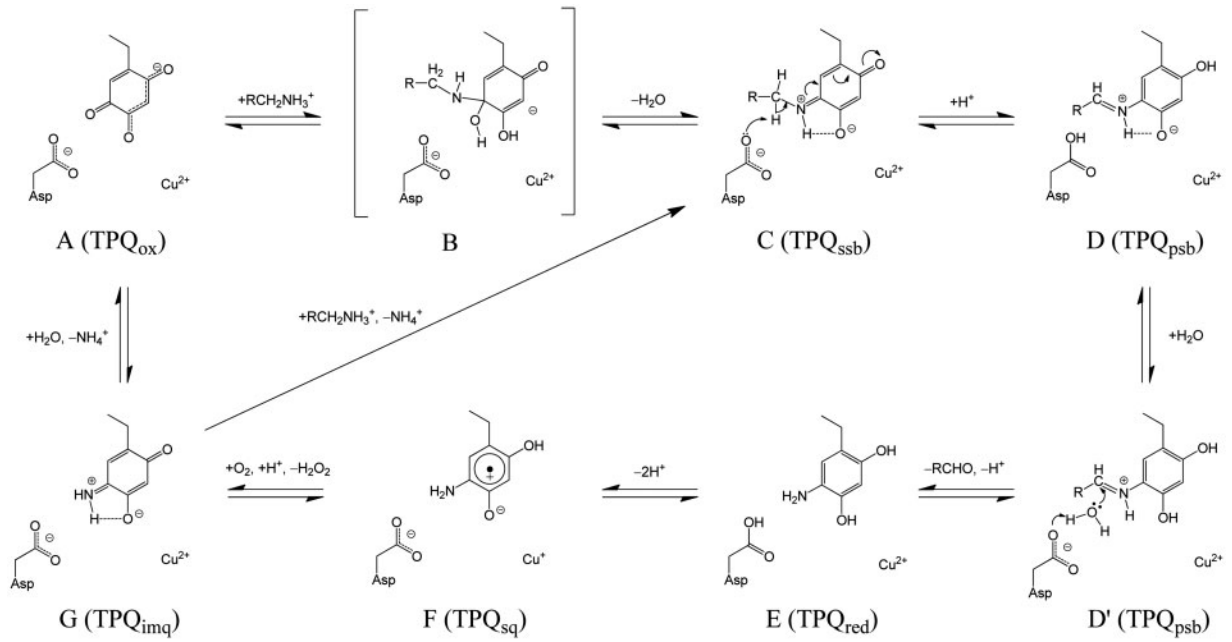

Scheme 1 Proposed reaction mechanism of CAO. The carbinolamine-like intermediate shown in parenthesis has not been structurally identified.

regenerate TPQ_{ox} via the semiquinone and iminoquinone forms of TPQ (TPQ_{sq} and TPQ_{imq}, respectively) with the concomitant release of hydrogen peroxide and ammonia (steps E → F → G → A) (*10*). Alternatively, under the steady-state conditions with excess substrate, TPQ_{ssb} is formed by direct transimination between TPQ_{imq} and the substrate (step G → C) (*11*). The bound copper ion plays an essential role in the oxidative half-reaction not only by mediating electron transfer from TPQ_{red} to O_2 but also by providing the binding site for reduced dioxygen species (O_2^-, HO_2^-, H_2O_2) (*6*, *10*).

In contrast to the virtually identical catalytic mechanism of CAOs commonly promoted by the cooperation of the TPQ cofactor, the conserved Asp residue, and the bound copper ion, substrate specificities differ considerably depending on the enzyme source. For example, the CAOs from *Escherichia coli* (ECAO) (*12*) and *Arthrobacter globiformis* (AGAO) (*13*) oxidize 2-phenylethylamine (PEA) and tyramine efficiently; however, benzylamine and ethylamine are not efficiently oxidized by these two enzymes. The enzyme from yeast *Hansenula polymorpha* (HPAO-1) preferentially acts on small aliphatic amines such as methylamine and ethylamine (*14*, *15*), whereas another isozyme from the same yeast (HPAO-2) shows distinct catalytic activity toward benzylamine (*16*). On the other hand, CAOs from bovine serum (BSAO) (*17*) and a plant *Pisum sativum* (*18*) efficiently catalyse the oxidation of long-chain aliphatic diamines, including spermidine. Structural bases for these substrate specificities have been provided for several CAOs, whose X-ray crystal structures are available. BSAO has a narrow substrate-binding pocket with a negatively charged residue at the entrance that should preferably bind a diamine substrate (*19*). A CAO from yeast *Pichia pastoris* has a shallow binding pocket suitable for short chain amines like methylamine (*20*). These structural features of the substrate-binding pocket may be reflected in the K_m values for each substrate. However, detailed investigation in view of the rate constants that could affect overall substrate specificities given by the second order rate constant, k_{cat}/K_m, has not been carried out, except for a recent kinetic and structural analysis of the substrate specificity of the two HPAO isozymes (*16*).

Hydrazine derivatives such as phenylhydrazine (PHZ) and benzylhydrazine (BHZ) are well-known irreversible inhibitors for CAOs as they form covalent complexes with the TPQ cofactor (*21-24*). Their reactions with TPQ are thought to be analogous to those of amine substrates, in which the C5 carbonyl group of TPQ undergoes nucleophilic attack by the deprotonated hydrazino group of the inhibitors to form a covalent adduct via a carbinolamine-like intermediate (Scheme 2) (*25*, *26*). However, the hydrazine derivatives have a nitrogen atom corresponding to the Cα atom of amines, which prevents abstraction of a proton at this position by the conserved Asp residue. Therefore, the enzyme is trapped as a TPQ/hydrazine adduct (*23*, *26*, *27*), which is a tautomeric mixture of hydrazone and azo forms, structurally analogous to TPQ_{ssb} and TPQ_{psb}, respectively.

In this paper, we report X-ray crystal structures of AGAO complexed with three hydrazine derivatives, BHZ, 4-hydroxybenzylhydrazine (4-OH-BHZ) and PHZ, which are structural analogues of PEA, tyramine and benzylamine, respectively (Fig. 1). The interactions of the amine substrates with the substrate-binding pocket of AGAO are expected to be similarly manifested in those of the corresponding hydrazine derivatives. Based on the results obtained, we provide structural insights into the substrate specificity of AGAO, which oxidizes PEA and tyramine as efficient substrates and benzylamine as a very poor substrate.

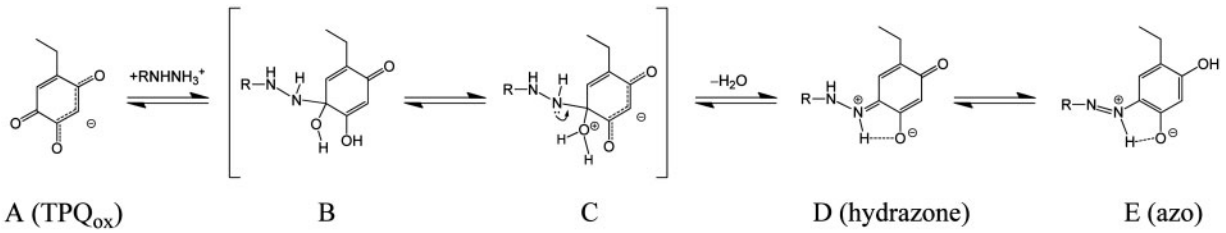

Scheme 2 Presumed reaction mechanism of hydrazine derivatives with TPQ.

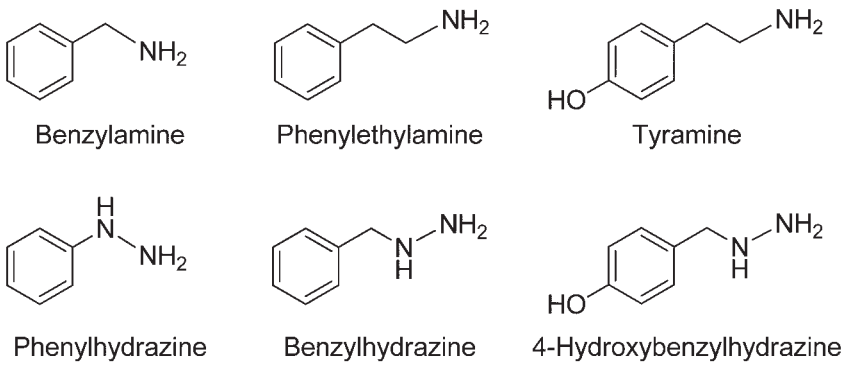

Fig. 1 Chemical structures of amine substrates and hydrazine derivatives used in this study.

Materials and Methods

Materials

AGAO was expressed in *E. coli* CD03 harbouring the expression plasmid pEPO-02, purified to homogeneity as a copper-depleted precursor form, and finally converted to the TPQ-containing mature form by incubation with excess copper ions, as described previously (*3*). Protein concentrations were determined by measuring the absorbance at 280 nm using an extinction coefficient of 13.2 for 1% (w/v) solution of the TPQ-containing form (*3*) and expressed as molar concentrations of the subunit, unless otherwise stated. PHZ was purchased from Nacalai Tesque (Kyoto, Japan); BHZ was from Aldrich (St. Louis, USA); and PEA was from Wako Pure Chemicals (Osaka, Japan). All other chemicals were of the highest grade commercially available.

Synthesis of 4-OH-BHZ

To a solution of 4-benzyloxyphenylmethanol (4.70 g, 21.9 mmol) in CH_2Cl_2 (50 ml), $SOCl_2$ (2.87 g, 24.1 mmol) was added at room temperature and the solution was refluxed for 1 h. After removal of excess $SOCl_2$ and the solvent by evaporation, the residue was dissolved in $CHCl_3$ (100 ml), and washed with saturated Na_2CO_3 and water. The organic layer was dried over Na_2SO_4 and concentrated *in vacuo* to give 4-benzyloxybenzyl chloride (3.47 g, 68%) as a brown oil; ^{1}H NMR ($CDCl_3$, 270 MHz) $\delta = 4.48$ (2H, s, -CH_2-Cl), 4.98 (2H, s, -CH_2-OPh), 6.87 (2H, d, $J = 8.3$ Hz, Ar), 7.21–7.35 (7H, m, Ar) ppm. A mixture of 4-benzyloxybenzyl chloride (2.32 g, 10 mmol), $N_2H_4 \cdot H_2O$ (5.0 g, 92.4 mmol), dioxane (10 ml) and ethanol (3 ml) was refluxed for 10 h. After removal of the solvent by evaporation, 10% HCl was added to the residue. The resulting precipitate was collected and washed with water. Recrystallization from 2-propanol yielded colourless needles of 4-benzyloxybenzylhydrazine hydrochloride (1.91 g, 72%); ^{1}H NMR (DMSO-d_6, 270 MHz) $\delta = 4.03$ (2H, s, -CH_2-$NHNH_2$), 5.00 (2H, s, -CH_2-OPh), 6.94 (2H, d, $J = 8.3$ Hz, Ar), 7.19–7.44 (7H, m, Ar) ppm. A solution of 4-benzyloxybenzylhydrazine hydrochloride (1.10 g, 4.80 mmol) in methanol (50 ml) was hydrogenated over 10% Pd/C (140 mg) at 2 atm overnight. After filtering the catalyst through Celite, the filtrate was evaporated and the residue was recrystallized from 2-propanol/ether to give colourless needles of 4-OH-BHZ hydrochloride (0.66 g, 79%); ^{1}H NMR (DMSO-d_6, 270 MHz) $\delta = 3.96$ (2H, s, -CH_2-$NHNH_2$), 6.78 (2H, d, $J = 8.3$ Hz, Ar), 7.23 (7H, d, $J = 8.3$ Hz, Ar) ppm.

Active-site titration with hydrazine derivatives

The reactivities of BHZ and 4-OH-BHZ with AGAO were determined by a spectrophotometric titration, as described previously for PHZ (*3*, *14*, *28*). Typically, 5 μM AGAO in 500 μl of 50 mM HEPES buffer, pH 6.8, was titrated by adding 2 μl aliquots of a 0.1 mM freshly prepared solution of each compound. After incubation at 30°C for at least 3 min to ensure the completion of the adduct formation, the increase in absorbance at 380 nm and 384 nm for BHZ and 4-OH-BHZ, respectively, was monitored with a spectrophotometer.

Stopped-flow measurements

Rapid UV/visible spectral changes of the reaction of AGAO with benzylamine in 50 mM HEPES buffer, pH 6.8, were monitored at 15°C using a stopped-flow spectrophotometer SX.17MV (Applied Photophysics, Leatherhead, UK). Typically, equal volumes (~30 μl each) of the enzyme solution (0.2 mM AGAO in 50 mM HEPES buffer, pH 6.8) and substrate solution (2 mM benzylamine) were mixed in a mixing cell (volume, 20 μl) triggered with an N_2-gas piston; the mixing dead time was generally 2.3 ms at an N_2-gas pressure of 500 kPa. UV/visible absorption spectra were recorded every 2.56 ms over the wavelength range of 250–800 nm. Spectral data were analysed using Pro-Kineticist II (Applied Photophysics) to resolve the spectra of the reaction intermediates and to calculate the rate constants for each reaction step. To avoid spectral changes associated with the oxidative half-reaction, both enzyme and substrate solutions were kept in a vacuum-type glove box SGV-65 V (AS ONE, Osaka, Japan) filled with 99.999% Ar gas for at least 6 h before the stopped-flow measurements.

X-ray crystallographic analysis

To complete the adduct formation with PHZ, BHZ and 4-OH-BHZ, an AGAO solution (final 0.15 mM subunit) was mixed with each hydrazine compound (final 0.3 mM) and incubated in a micro test tube at 37°C for 12 h before crystallization. After dialysis to remove the unreacted hydrazine, the enzyme was crystallized by the micro dialysis method as described previously (*7*). The protein solution was placed in a 50-μl dialysis button and dialysed at 16°C against 1.05 M potassium–sodium tartrate in 25 mM HEPES buffer, pH 6.8. After sufficient growth of the crystals, the dialysis buttons were transferred into the new reservoir solution supplemented with 45% (v/v) glycerol at 16°C for 24 h as a cryoprotectant. The crystals were mounted on thin nylon loops (ϕ, 0.4–0.5 mm) and

frozen by flash cooling to 100 K in cold N_2 gas stream. Before exposure to the X-rays, the UV/visible absorption spectra of the crystals were analysed by single-crystal micro-spectroscopy at 100 K (*7*, *9*). The micro-spectrophotometer system consisted of a deuterium tungsten halogen light DT-MINI (Ocean Optics, FL, USA), Cassegrainian mirrors (Bunkoh-Keiki Co. Ltd. Tokyo, Japan), an optical fibre and a linear CCD-array spectrometer SD2000 (Ocean Optics). Absorption spectra were recorded over the wavelength range of 178–879 nm and corrected for the air blank baseline and dark reference.

Diffraction data sets were collected at 100 K with the synchrotron X-radiation ($\lambda = 0.9$ Å) using an imaging plate, DIP6040 (Bruker AXS, Yokohama, Japan) in the station BL44XU at the SPring-8 (Hyogo, Japan). The collected data was processed and scaled using MOSFLM (*29*) and SCALA in CCP4 (*30*), respectively. The crystals of AGAO reacted with BHZ (AGAO/BHZ) and 4-OH-BHZ (AGAO/4-OH-BHZ) were found to belong to the space group *I*2, which is identical to the AGAO crystals determined under the cryo conditions and contains the dimer molecule in the asymmetric unit (*6*) (PDB accession code, 1IU7). The crystals of AGAO reacted with PHZ (AGAO/PHZ) belonged to the space group *C*2, which is identical to those of the precursor AGAO (apo form) determined at an ambient temperature and contains a single subunit in the asymmetric unit (*31*) (1AVK). For the phase determination, molecular replacement was performed using a homo dimer model in AGAO/BHZ and AGAO/4-OH-BHZ and a monomer model in AGAO/PHZ. The wild-type AGAO structure (1IU7) without solvent molecules was used as a search model for molecular replacement for AGAO/BHZ and AGAO/4-OH-BHZ with TPQ382 being replaced with an unmodified Tyr residue, whereas the precursor structure (1AVK) was used without any modification for AGAO/PHZ. The program used for molecular replacement, refinements, calculation of the electron-density maps and assignment of solvent molecules was CNS Version 1.1 (*32*). Manual rebuilding was performed using an xfit module in an XtalView software package (*33*). Following rigid-body refinement, the initial structures of the AGAO/PHZ, AGAO/BHZ and AGAO/4-OH-BHZ were further refined through simulated annealing with a slow cooling protocol from 2500 to 300 K at 25 K-drop per cycle, and several cycles of B-factor and positional refinements. In the modelling stage, the models of the TPQ-hydrazine complexes were built for hydrazone and azo forms using Insight II (Accelrys, CA, USA), and then topology and parameter files for refinement used for CNS were generated with XPLO2D in the X-UTIL package (*34*). The residue 382 was replaced by a complex of TPQ-BHZ, TPQ-4-OH-BHZ, or TPQ-PHZ, and the conformation was adjusted on the basis of the $2F_o-F_c$, F_o-F_c, and omit maps. These models were refined further through several cycles of B-factor and positional refinements after introducing solvent molecules followed by manual modelling with xfit. The quality of the structure was validated with MolProbity (*35*). The details and statistics of the data processing and crystallographic refinements are summarized in Table 1. The atomic coordinates and structure factors for the AGAO/BHZ, AGAO/4-OH-BHZ and AGAO/PHZ have been deposited in the Protein Data Bank Japan at the Institute for Protein Research, Osaka University (PDBj; http://www.pdbj.org/) with the accession codes 2E2V, 2E2U and 2E2T, respectively.

Results

Transient-state kinetic analysis with benzylamine

We previously determined the substrate specificity of AGAO by using various amine substrates (*9*, *13*). In general, substrates with an aromatic (or heterocyclic) ring at an opposite end of the aliphatic amino group were found to be good substrates for AGAO with large k_{cat}/K_m values. However, benzylamine, which also contains a benzene ring, served as a very poor substrate ($K_m = 100\,\mu M$, $k_{cat} = 0.24\,s^{-1}$) as compared to PEA ($2.5\,\mu M$, $44\,s^{-1}$) and tyramine ($10.4\,\mu M$, $35\,s^{-1}$) when measured at 15°C (*7*, *9*, *36*). Since the first reaction product aldehyde from these substrates containing the distal aromatic ring is released in the former reductive half-reaction and therefore the latter oxidative half-reaction should proceed irrespectively of the amine substrates (Scheme 1), the low reactivity of benzylamine, particularly in view of its small k_{cat} value, may be ascribed to a lowered reaction rate(s) in a step(s) of the reductive half-reaction. To identify the reaction step(s) accounting for the markedly decreased

Table I. Statistics of data collection and crystallographic refinement.

	AGAO/BHZ	AGAO/4-OH-BHZ	AGAO/PHZ
Data collection			
Temperature (K)	100	100	100
Wavelength (Å)	0.9	0.9	0.9
Space group	*I*2	*I*2	*C*2
Unit cell dimensions			
a, *b*, *c* (Å),	158.05, 62.64, 183.95	157.97, 63.07, 184.05	157.64, 63.08, 91.86
β (deg)	112.16	112.04	112.16
No. of observations	652,680	720,500	329,900
No. of unique reflections	175,433	189,031	87,299
Multiplicity	3.7	3.8	3.8
$d_{max}-d_{min}$ (Å)	26.5–1.72	26.6–1.68	26.5–1.73
Overall completeness (%)	99.2	98.9	100.0
Overall R_{merge} (%)[a]	7.1	5.8	5.7
Refinements			
$d_{max}-d_{min}$ (Å)	26.5–1.80	26.6–1.68	26.5–2.05
No. of solvent atom	1205	1218	318
RMS deviation from ideal values[b]			
Bond lengths (Å)	0.006	0.005	0.005
Bond angles (deg)	1.38	1.35	1.36
Residual *R* (%)[c]	21.7	20.9	20.5
Free residual *R* (%)[d]	25.2	23.6	24.3
Fraction of data in R_{free} set (%)	5	5	5
Ramachandran plot			
Favoured/allowed/outlier (%)	96.3/3.5/0.2	96.0/3.8/0.2	95.8/4.0/0.2

[a]$R_{merge} = \Sigma h\ \Sigma i\ |I_{h,i} - \langle I_h \rangle| \ /\ \Sigma h\ \Sigma i\ I_{h,i}$, where $I_{h,i}$ is the intensity value of the *i*th measurement of *h* and $\langle I_h \rangle$ is the corresponding mean value of I_h for all *i* measurements. [b]RMS deviation from ideal values were calculated with CNS. [c]$R = \Sigma||F_o| - |F_c|| \ /\ \Sigma|F_o|$. [d]Free residual *R* is an *R* factor of the CNS refinement evaluated for 5% of the reflections that were excluded from the refinement.

reactivity of benzylamine, we conducted a transient-state kinetic analysis of the reductive half-reaction with benzylamine under single-turnover conditions.

Upon anaerobic mixing of AGAO with excess benzylamine, the TPQ_{ox}-derived absorption band at 480 nm slightly decreased with a concomitant peak shift to 460 nm within 50 ms (Fig. 2A). An additional shoulder band appeared around 310 nm. In the following phase (from 50 ms to 3.0 s), the absorption band at 460 nm increased again and a shoulder band ~340 nm increased (Fig. 2B). In the final phase (from 3.0 to 16.0 s), the species with a shoulder band ~340 nm and with a λ_{max} at about 460 nm is gradually converted to a new species with absorption peaks at 365, 438 and 465 nm, assignable to TPQ_{sq} (Fig. 2C) (*6*, *37*). Isosbestic points of the spectra were observed at 400 and 525 nm in the initial phase (Fig. 2A) and at 540 nm in the intermediary phase (Fig. 2B), indicating that the reductive half-reaction with benzylamine proceeds with multiple intermediates. Although these spectral changes apparently differ from those observed in the reactions with PEA (*7*) and tyramine (*36*), the same model has been applied to the oxidation of benzylamine in solving the mechanism by global analysis of the spectral changes. The multi-wavelength data of spectral changes with benzylamine were therefore fitted to the four-step model (Scheme 3) (*7*, *36*), where the absorption spectrum of apo AGAO (without TPQ) was used as that of TPQ_{red}, assuming that TPQ_{red} exhibits no absorption >300 nm (*25*). In the data fitting, the absorption spectra of TPQ_{ox} and TPQ_{red} were fixed, whereas the spectra of other species and rate constants at all steps were varied until a reasonable solution was finally obtained. Shown in Fig. 2D and 2E are the deconvoluted UV/visible absorption spectra and the time courses of concentration changes of TPQ_{ox}, TPQ_{ssb}, TPQ_{psb}, TPQ_{red} and TPQ_{sq}. The absorption

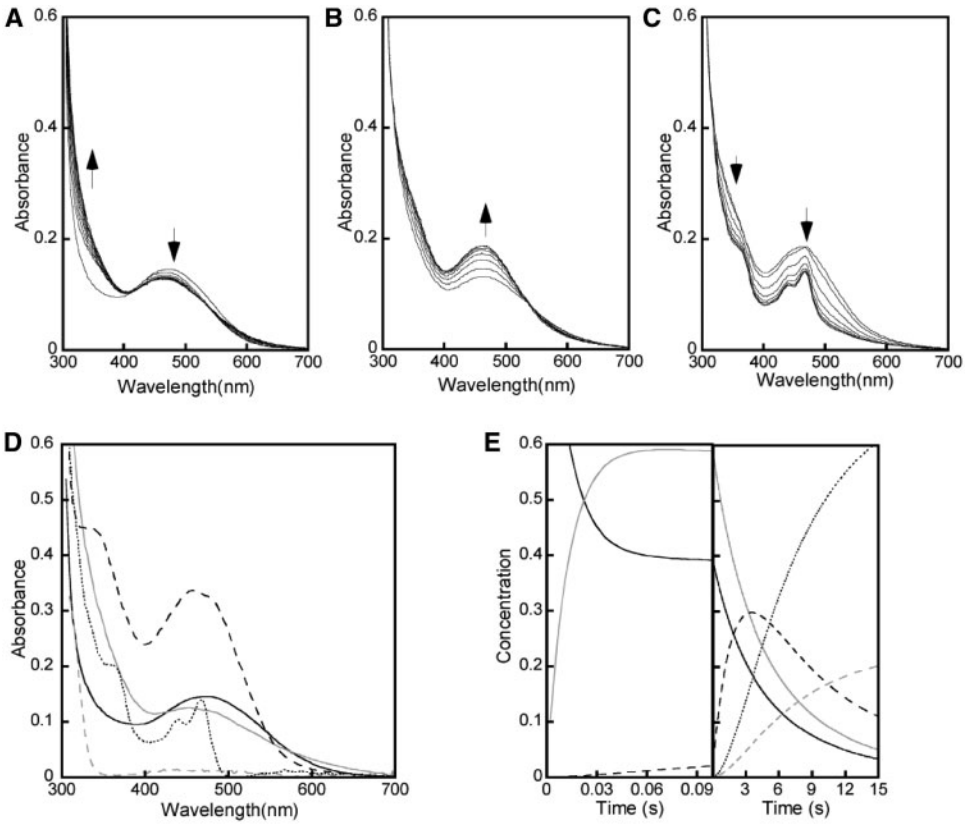

Fig. 2 Spectral changes during the reductive half-reaction of wild-type AGAO reacted with benzylamine. (A) UV/visible absorption spectra were recorded after mixing AGAO (0.1 mM subunit) with 1.0 mM benzylamine in 50 mM HEPES buffer, pH 6.8, at 15°C under anaerobic conditions. The spectra obtained at (**A**) 0, 2.3, 6.4, 12, 17, 22, 27, 32, 37, 42 and 47 ms, (B) 0.1, 0.4, 0.8, 1.2, 1.6, 2.0, 2.6 and 3.0 s, and (C) 3, 4, 6, 8, 10, 12, 14 and 16 s are shown. Arrows indicate the direction of the spectral changes. Deconvoluted absorption spectra (D) and the time course of the concentration changes of each intermediate (E) are shown for TPQ_{ox} (black solid), TPQ_{ssb} (gray solid), TPQ_{psb}, (black dashed), TPQ_{red} (gray dashed) and TPQ_{sq} (black dotted).

$$TPQ_{ox} \underset{k_{-1}}{\overset{k_{+1}}{\rightleftharpoons}} TPQ_{ssb} \underset{k_{-2}}{\overset{k_{+2}}{\rightleftharpoons}} TPQ_{psb} \underset{k_{-3}}{\overset{k_{+3}}{\rightleftharpoons}} TPQ_{red} \underset{k_{-4}}{\overset{k_{+4}}{\rightleftharpoons}} TPQ_{sq}$$

Scheme 3 Kinetic mechanism of the reductive-half reaction applied for global analysis of spectral changes.

spectrum obtained for TPQ_{ssb}, with a broad and weak absorption >400 nm, resembles that of a model compound in a non-polar (CH_2Cl_2) or polar (CH_3CN) aprotic solvent (*25*). The spectrum obtained for TPQ_{psb} shows a broad peak at 460 nm with a higher absorption coefficient. This absorption band considerably red-shifted compared with those formed with PEA and tyramine ($\lambda_{max} = 410$ mm), probably due to the wide resonance system extended from the TPQ ring to the benzene ring of the substrate (*cf.* Scheme 1, D, where $R = C_6H_5$). The calculated spectrum for TPQ_{sq} with absorption peaks at 360, 438 and 467 nm agrees well with those obtained for the reductive half-reaction with PEA and tyramine as substrates. The substrate-independent spectrum of TPQ_{sq} is reasonable, because TPQ_{sq} is formed after the hydrolysis of TPQ_{psb} and the release of the first product aldehyde in the reductive half-reaction (Scheme 1).

Rate constants for the reaction with benzylamine obtained by global analysis are summarized in Table 2, together with those determined previously for the reactions with PEA (*7*) and tyramine (*36*). Significant differences were observed for all rate constants except for k_{+4} and k_{-4}. In particular, rate constants of the proton abstraction step (k_{+2}, $TPQ_{ssb} \rightarrow TPQ_{psb}$) and its reverse ($k_{-2}$), and also the step of TPQ_{psb} hydrolysis (k_{+3}, $TPQ_{psb} \rightarrow TPQ_{red}$) and its reverse ($k_{-3}$) are 10^2–10^3 orders of magnitude smaller than those for PEA and tyramine, indicating that the decreases in these rate constants are presumably associated with the low reactivity of benzylamine. The two steps appear to be rate-limiting for the overall reaction with benzylamine as the steady-state k_{cat} value (0.24 s^{-1}) (*9*) is comparable with the k_{+2} and k_{+3} values. The rate constant of the $TPQ_{ox} \rightarrow TPQ_{ssb}$ step (k_{+1}) is also 10- to 15-fold smaller in the reaction with benzylamine than the reactions using PEA and tyramine as the substrates. In contrast, the rate constant of the $TPQ_{red} \rightarrow TPQ_{sq}$ step (k_{+4}) is similar between the three substrates, and this observation is again consistent with this step proceeding after the release of the product aldehyde and being independent of amine substrate used.

Table II. Kinetic constants of each step of the reductive half-reaction determined at 15°C[a].

	Benzylamine[b]	PEA[c]	Tyramine[d]
k_{+1} (s^{-1})	48	699 ± 75	601 ± 4.7
k_{-1} (s^{-1})	32	201 ± 26	165 ± 7.1
k_{+2} (s^{-1})	0.405	411 ± 6.0	250 ± 8.0
k_{-2} (s^{-1})	0.089	111 ± 9.4	57 ± 4.3
k_{+3} (s^{-1})	0.31	197 ± 18	108 ± 0.58
k_{-3} (s^{-1})	0.074	282 ± 106	47 ± 11
k_{+4} (s^{-1})	71	93 ± 120	83 ± 17
k_{-4} (s^{-1})	24	43 ± 28	43 ± 8.1

[a]Reactions were analysed according to Scheme 3. [b]SD values for all kinetic constants were <0.005 s^{-1} after the Levenberg–Marquardt minimization. [c]Adopted from Chiu *et al.* (*7*). [d]Adopted from Murakawa *et al.* (*36*).

X-ray crystal structure of AGAO reacted with hydrazine derivatives

To elucidate the interactions of the active-site residues with the hydrazine adducts, and thereby decipher those with the reaction intermediates formed from the corresponding amine substrates, X-ray crystal structures of the complexes thoroughly reacted with the hydrazine derivatives were determined. Three hydrazine derivatives, BHZ, 4-OH-BHZ and PHZ, which are regarded as structural analogues for PEA, tyramine and benzylamine, respectively, were used in this study (Fig. 1). Prior to crystallization, the reactivities of these hydrazine derivatives with AGAO were examined in solution by spectrophotometric titration; the TPQ/hydrazine adducts are known to exhibit intense and characteristic absorption bands in the visible region (*21–24*). Previously, the titration of AGAO with PHZ gave 0.63 mol of PHZ reacted with 1 mol of the AGAO subunit (*7*). Similar results were obtained for the titration with BHZ (0.64 mol/mol) and 4-OH-BHZ (0.78 mol/mol) in the present study. Reaction of <1 mol of hydrazine derivatives per mol of subunit has often been observed for many CAOs and ascribed to a half-of-the-site reactivity of the enzyme dimer (*22*, *38*). However, structural evidence for the active-site cooperativity between the two subunits of the dimer has not been obtained for any CAOs including AGAO. It is possible that the less-than-stoichiometric reactivities of hydrazine derivatives are derived from the conformational flexibility of the TPQ cofactor fluctuating between the productive (active) 'off-copper' and non-productive (inactive) 'on-copper' forms (*15*, *26*, *39–42*).

Crystals of AGAO complexed with BHZ, 4-OH-BHZ and PHZ exhibited a deep yellow colour with absorption maxima at 387, 375 and 435 nm, respectively (Fig. 3), which are essentially identical with those measured in solution as described above. The crystals were then subjected to X-ray diffraction analyses. As summarized in Table 1, all crystals of the AGAO/BHZ, AGAO/4-OH-BHZ and AGAO/PHZ adducts diffracted to ~1.7-Å resolution and therefore the diffraction data were further processed to structure refinements.

After several cycles of initial refinements of the AGAO/BHZ structure, the $F_o - F_c$ omit map around residue 382 (TPQ) clearly showed an extra electron density connected to the C5 position of TPQ, indicating the presence of a covalently-linked hydrazine derivative. The structure of the hydrazine adduct was modelled on the basis of the $2F_o - F_c$ and $F_o - F_c$ maps and also the $F_o - F_c$ omit map. It has been reported that hydrazine derivatives form a covalent adduct with TPQ in either a hydrazone (N2–N1 = C5; Fig. 4A) or azo (N2 = N1–C5; Fig. 4B) form (*25*, *26*). To identify the predominant form in the AGAO/BHZ structure, both azo and hydrazone models were examined for fitting to the electron density map. After several cycles of independent refinements using the two models, R and R_{free} values decreased to essentially identical values (21.7% and 25.2%, respectively) for both models (Table 1). Although the two models similarly fitted to the

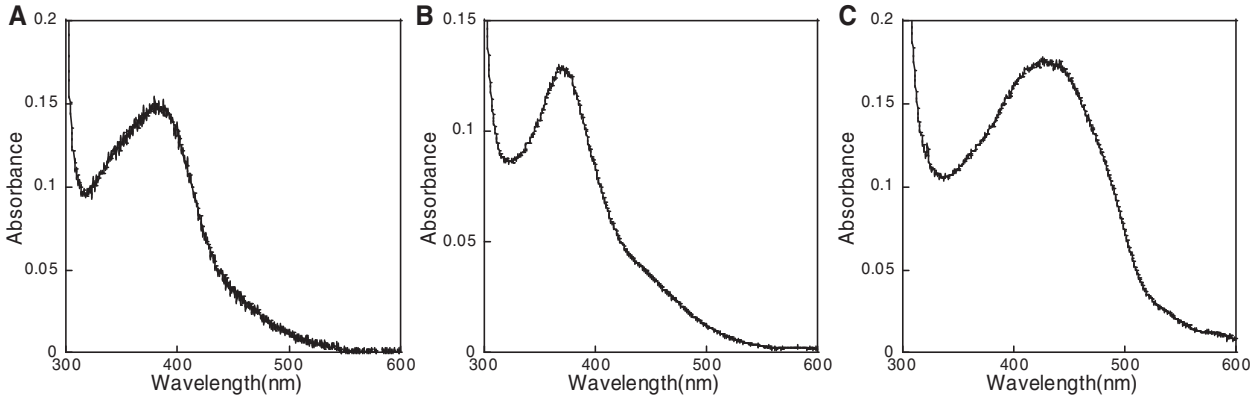

Fig. 3 Absorption spectra of crystals of AGAO/hydrazine adducts. UV/visible absorption spectra were measured for the single crystals (~0.2 × 0.4 × 0.1 mm) of the (A) AGAO/BHZ, (B) AGAO/4-OH-BHZ and (**C**) AGAO/PHZ adducts.

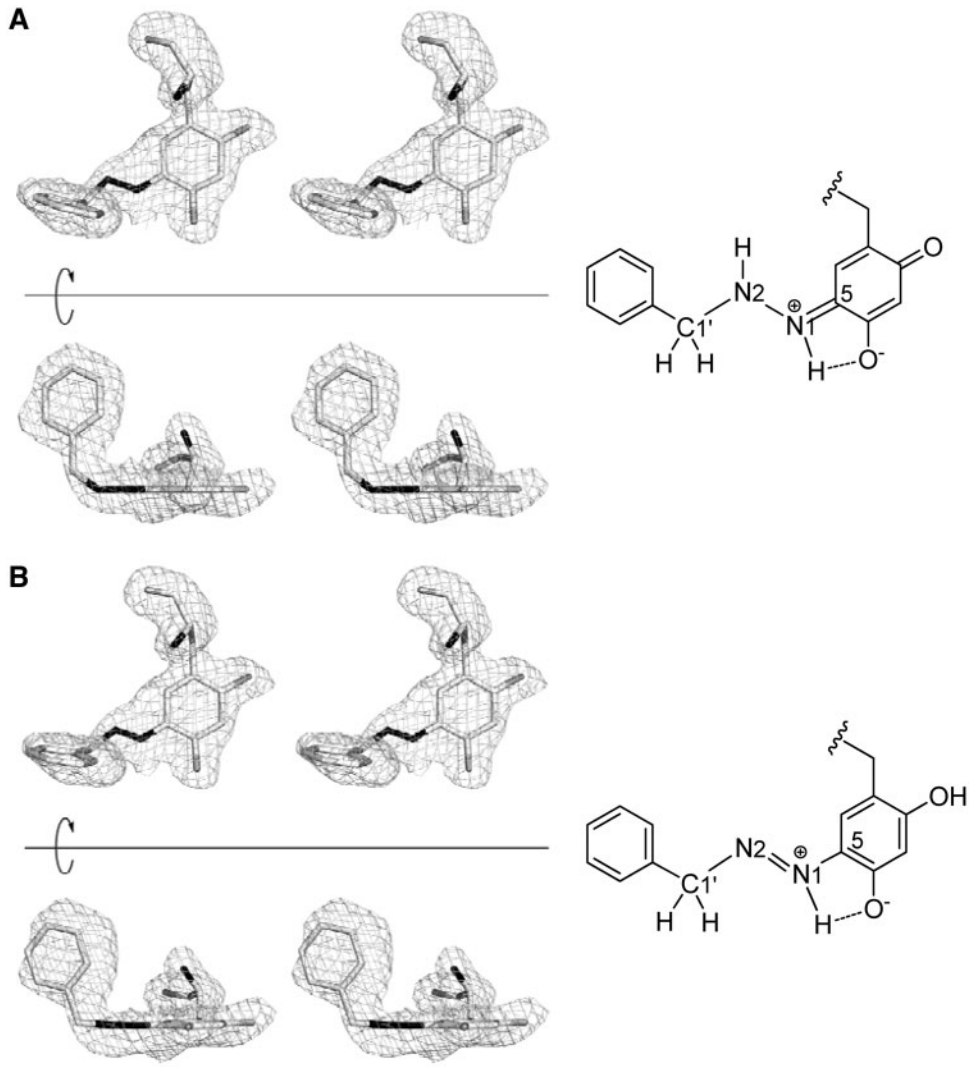

Fig. 4 X-ray crystal structure of the TPQ/BHZ adduct. Stereo diagrams of the refined models of the hydrazone form (A) and the azo form (B) of the TPQ/BHZ adduct are shown with an annealed $F_o - F_c$ omit map contoured at 4.4 σ. Upper and lower panels are the views from two different directions by a 90° rotation. Chemical structures for the hydrazone and azo forms are depicted on the right.

electron density map, close inspection of the aromatic ring of BHZ in a view parallel to the TPQ ring revealed that the hydrazone model fits better to the $F_o - F_c$ omit map than the azo model (Fig. 4A and B, *lower panels*). The C1′, N1 and N2 atoms are also better accommodated to the electron density in the hydrazone model than in the azo model. Collectively, the structure refinement strongly suggests that the hydrazone form is predominant in the crystal of the AGAO/BHZ adduct.

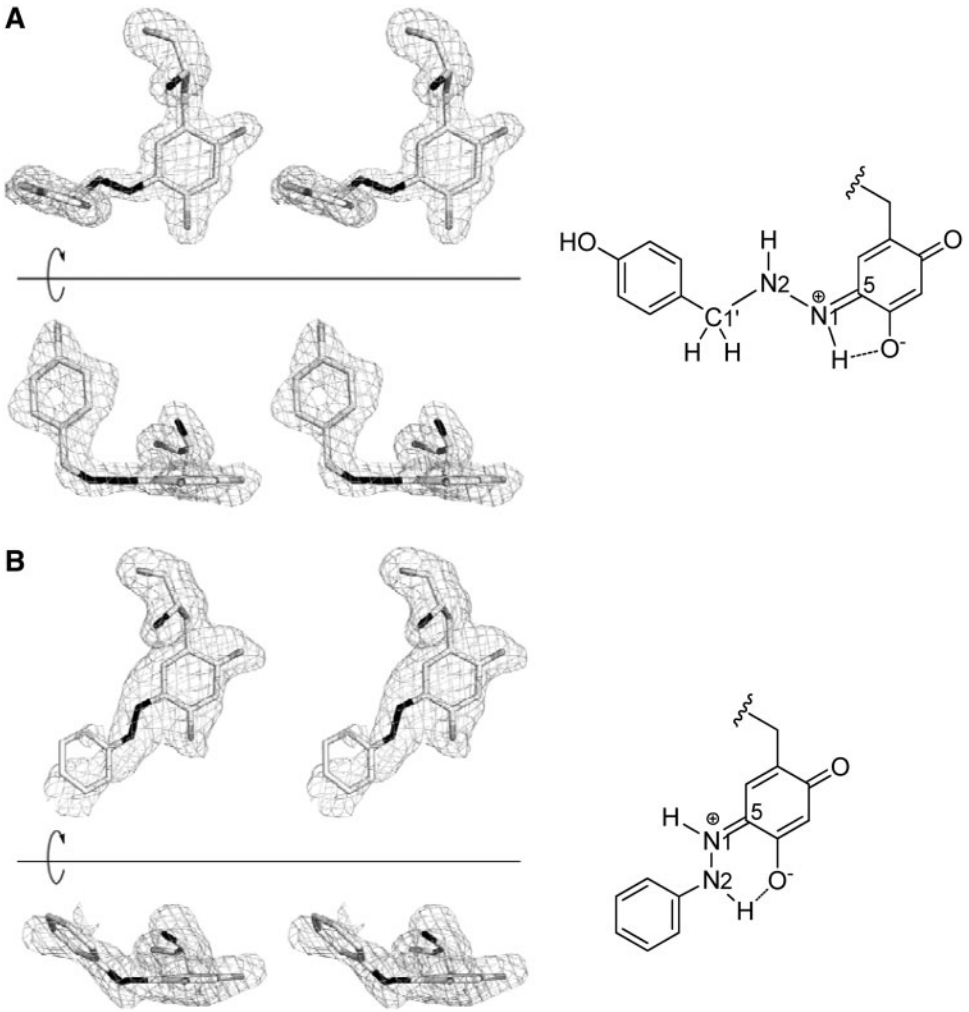

Fig. 5 X-ray crystal structures of the TPQ/4-OH-BHZ and TPQ/PHZ adducts. Stereo diagrams of the refined models of the hydrazone forms of the TPQ/4-OH-BHZ adduct (A) and the TPQ/PHZ adduct (B) are shown with an annealed $F_o - F_c$ omit map contoured at 4.4 σ. Upper and lower panels are the views from two different directions by a 90° rotation. Chemical structures for the hydrazone form are depicted on the right.

Similarly, structure refinements for the AGAO/4-OH-BHZ adduct have revealed that the hydrazone form is the major tautomer (Fig. 5A). Comparison of the structures of AGAO/BHZ and AGAO/4-OH-BHZ adducts indicated that the aromatic rings of both inhibitors occupy the same position in the active site of AGAO, as described later. In contrast, in the crystal structure of the AGAO/PHZ adduct, the electron density in the $F_o - F_c$ omit map was rather poor for the aromatic ring of the inhibitor (Fig. 5B, *upper panel*). If the predominant tautomer is an azo form (analogous to TPQ_{psb}), the inhibitor/quinone moiety has a fully conjugated system and the aromatic ring of PHZ and the quinone ring of TPQ should adopt a coplanar conformation (*43*). However, the electron density corresponding to the aromatic ring of BHZ tilts upward about 45° against the remaining part of the electron density containing the quinone ring of TPQ (Fig. 5B, *lower panel*), indicating that the coplanar azo form is less feasible. Thus, it was concluded that the hydrazone form is also predominant in the crystal structure of the AGAO/PHZ adduct. It is noteworthy that in the best-fit model of the hydrazone form of the AGAO/PHZ adduct, the hydrogen at the N2 atom but not at the N1 atom is hydrogen-bonding with the C4 oxygen atom of the TPQ ring to form a six-member ring (Fig. 5B). Finally, the overall structures of the AGAO/PHZ, AGAO/BHZ and AGAO/4-OH-BHZ adducts all refined in the hydrazone forms are essentially identical with the structure of the wild-type, ligand-free AGAO (PDB: 1IU7) (*6*), with root mean square deviations for the main-chain atoms of 0.43, 0.19 and 0.14 Å, respectively.

Discussion

In this study, we have determined the crystal structures of AGAO complexed with three hydrazine derivatives, BHZ, 4-OH-BHZ and PHZ. The X-ray structural data suggest that all the AGAO/hydrazine adducts occur predominantly in a hydrazone form that is structurally analogous to TPQ_{ssb}. The crystal structure of the AGAO/BHZ adduct has already been reported by another group (PDB: 1W5Z), but without particular

discussion with regard to the substrate specificity of AGAO (*44*). The previously and presently reported structures of the AGAO/BHZ adduct are virtually identical with each other despite significant differences in the preparations of recombinant AGAO (strep-tagged or non-tagged), the conditions for adduct formation (crystal soaking or pre-reacted in solution), and the space groups of the crystals obtained (*C*2 or *I*2). Furthermore, the crystal structure of ECAO complexed with 2-hydrazinopyridine (2-HP) has been reported, in which the hydrazone tautomer is also predominant (*26*). In the crystal structure of the ECAO/2-HP adduct, the hydrazone form appeared to be stabilized by two hydrogen-bonding interactions between the TPQ/2-HP moiety and two active-site residues: the catalytic base (Asp383, corresponding to Asp298 in AGAO) and the conserved tyrosine residue (Tyr369, corresponding to Tyr284 in AGAO) (*26*). The latter hydrogen bond is also found in the structures of the AGAO/hydrazine adducts (Fig. 6). However, there is no hydrogen-bonding interaction between the aromatic ring of the hydrazine derivatives and the catalytic base (Asp298) of AGAO. Instead, hydrophobic interactions between the aromatic ring of the bound inhibitors and the amino acid residues constituting the substrate-binding pocket presumably play an important role in stabilizing the hydrazone form, as described below.

The active-site structures of the ligand-free AGAO and three AGAO/hydrazine adducts (AGAO/PHZ, AGAO/BHZ and AGAO/4-OH-BHZ) are compared in Fig. 6. It is clearly seen that the aromatic ring of BZH and 4-OH-BHZ is tightly bound in the substrate-binding pocket by hydrophobic interactions with the side-chains of Tyr302, Leu137, Tyr307, Phe105, Pro136, Ala135, Leu358, Trp359, Trp168 and Phe407 (Leu358 and Trp359 are derived from the neighboring subunit of the dimer) (in the order shown in Fig. 6, clockwise from Tyr302), and held nearly perpendicular against the TPQ ring with a dihedral angle of ~85° for the planes formed by the N1-N2-C1′-C2′ atoms (see also Figs 4A and 5A). Furthermore, the binding of the aromatic ring of 4-OH-BHZ is stabilized by hydrogen bonds between the 4-OH group and two water molecules (Wat2 and Wat3) contained in the hydrophobic cavity, where Wat2 is also hydrogen bonding with Wat1 which is further interacting with the carboxyl group of Asp357 (Fig. 6). Wat1 and Wat2 have also been observed in the ligand-free AGAO structure (PDB: 1IU7) (*6*). These hydrophobic and hydrogen-bonding interactions are essentially identical with those observed in the intermediates (TPQ_{ssb}) of a catalytic-base mutant (D298A) of AGAO formed in the reaction with PEA and tyramine (*7*, *36*). Altogether, the aromatic rings of both BZH and 4-OH-BHZ are accommodated inside the hydrophobic cavity of the substrate-binding pocket in a well-defined conformation (Fig. 7). The substrate-binding pocket is located at the bottom of the funnel-shaped substrate channel (*31*, *45*). In marked contrast to the aromatic rings of BHZ and 4-OH-BHZ, hydrophobic interactions of the aromatic ring of PHZ appear to be only partially at one side and near the end of the substrate-binding pocket in the structure of the AGAO/PHZ adduct (Fig. 7). The poor electron density in the $F_o - F_c$ omit map (Fig. 5B) also suggests an undefined conformation of the aromatic ring of PHZ,

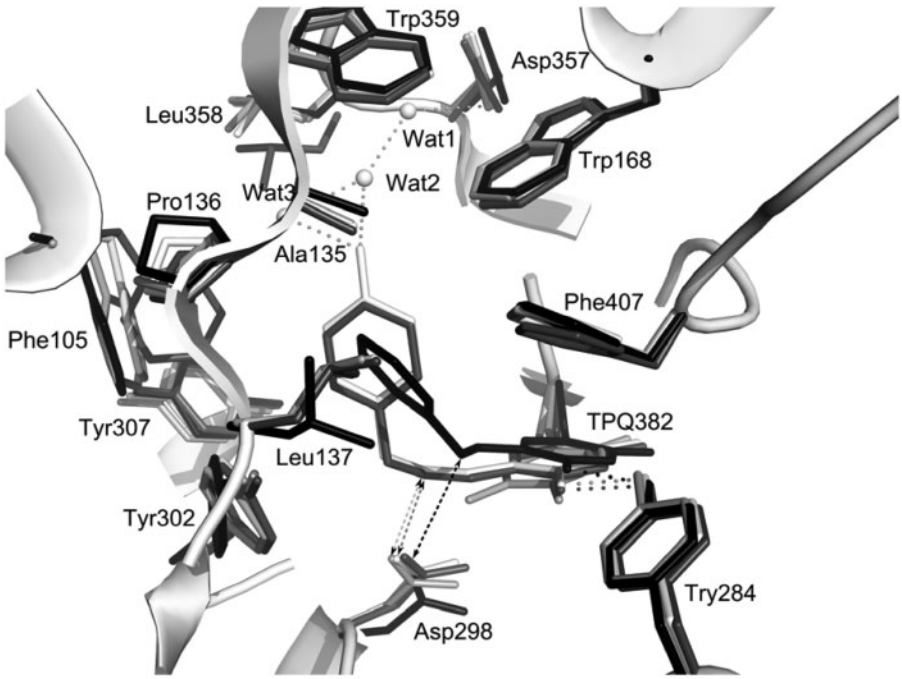

Fig. 6 Comparison of the active-site structures. Active-site structures of the ligand-free AGAO (pale gray), AGAO/PHZ (black), AGAO/BHZ (dark gray) and AGAO/4-OH-BHZ (white) adducts are superimposed in stick models. Broken arrows represent the distance between an oxygen atom of the carboxyl group of Asp298 and the N2 atoms of PHZ, BHZ and 4-OH-BHZ. Three water molecules (Wat1, Wat2 and Wat3) identified in the substrate-binding pocket of the AGAO/4-OH-BHZ adduct are shown as small spheres. Dotted lines represent hydrogen bonds.

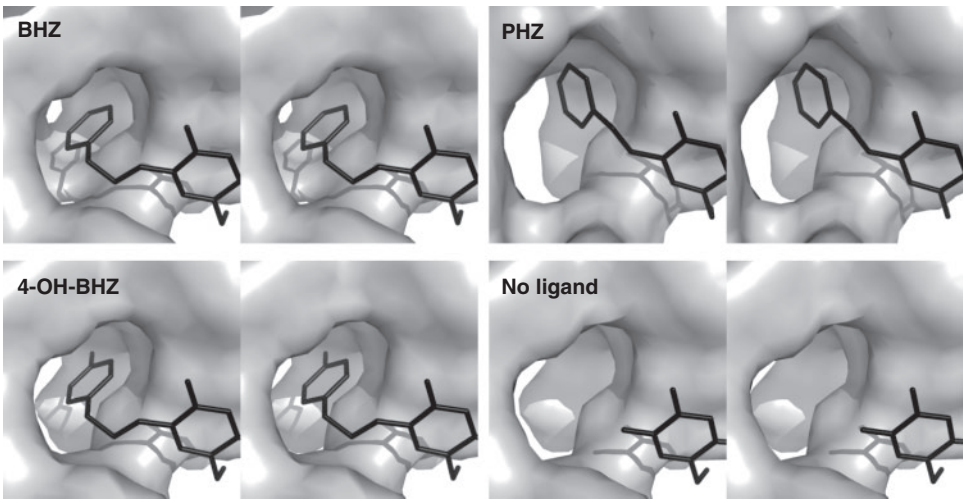

Fig. 7 Comparison of the surfaces of the hydrophobic cavity of the substrate-binding pocket. The surfaces of the hydrophobic cavity of the substrate-binding pocket are shown in stereo for the AGAO/BHZ (BHZ), AGAO/4-OH-BHZ (4-OH-BHZ), AGAO/PHZ (PHZ) adducts and the ligand-free AGAO (No ligand). Bound inhibitors are shown by stick models.

even though the hydrazone form has been assigned as the major tautomer. It is interesting to note that in the structures of the AGAO/hydrazine adducts, several residues constituting the substrate-binding pocket have conformations different from those in the structure of ligand-free enzyme (Fig. 6). Namely, in the AGAO/BHZ and AGAO/4-OH-BHZ structures, the side chains of Tyr302, Tyr307, Phe105 and Leu358 moved closer to the aromatic ring of the inhibitors and as a result the hydrophobic cavity became narrower than that of the ligand-free enzyme (Fig. 7). Vice versa, the residues Pro136, Phe105 and Leu137 in the AGAO/PHZ structure have moved to make the cavity even wider than the ligand-free enzyme (Fig. 7). These findings strongly suggest that the substrate-binding pocket of AGAO is formed, at least partially, by an induced-fit movement of those residues upon binding of the substrates (inhibitors).

Structural comparison of the AGAO/hydrazine adducts provides another important feature of the active site. As the result of the binding of the inhibitor aromatic rings to the hydrophobic pocket near the TPQ cofactor, distances between the side-chain carboxyl group of the catalytic base (Asp298) and the N2 atom of the TPQ/hydrazine adducts are also fixed; they were estimated to be 2.86, 3.06 and 5.76 Å in the AGAO/BHZ, AGAO/4-OH-BHZ and AGAO/PHZ adducts, respectively (Fig. 6). The distances of 2.86 and 3.06 Å suggest the presence of hydrogen bonds between the deprotonated carboxyl group of Asp298 and the N2 hydrogen atom in the hydrazine forms of the AGAO/BHZ and AGAO/4-OH-BHZ adducts. Clearly, the distance in the AGAO/PHZ adduct is about twice as long when compared with the distances in the AGAO/BHZ and AGAO/4-OH-BHZ adducts. As described above, the TPQ/hydrazone can be regarded as a structural analogue of TPQ_{ssb} formed in the reaction with the corresponding amine substrates, which is difficult to capture crystallographically unless a catalytic-base mutant (D298A) is used (*7*, *36*). The N2 atom of the TPQ/hydrazine adducts corresponds to the Cα atom of TPQ_{ssb}. Thus, the distances between the carboxyl group of Asp298 and the N2 atom of hydrazone would represent those between the proton donor (TPQ_{ssb}) and acceptor (the carboxyl group of Asp298) in the catalytic intermediate and may be correlated with the catalytic efficiencies of the substrate amines.

As determined by transient-state kinetic analysis, the rate constant of the proton abstraction step (k_{+2}, $TPQ_{ssb} \rightarrow TPQ_{psb}$) in the reaction with benzylamine is slower by $\sim 10^3$-fold than those with PEA and tyramine (Table 2). We previously reported that the proton abstraction step is driven by quantum mechanical proton tunnelling in the reductive half-reaction of AGAO with both PEA and tyramine (*36*). As the tunnelling is highly dependent on the width and height of the energy barrier, which is closely correlated with the proton donor-to-acceptor distance, it is predicted that the contribution of the tunnelling in the reaction with benzylamine, with a longer proton donor-to-acceptor distance, is very small as compared with those of PEA and tyramine. Although the extent of the contribution of proton tunnelling in the reaction with benzylamine has not been determined, the significantly small rate constant (k_{+2}) at the proton abstraction step ($TPQ_{ssb} \rightarrow TPQ_{psb}$) is most likely derived from the longer distance between the carboxyl group of Asp298 and the Cα atom of TPQ_{ssb} (N2 atom of hydrazone).

The hydrolysis rate of the benzylamine-derived TPQ_{psb} (k_{+3}, $TPQ_{psb} \rightarrow TPQ_{red}$) is also slower by several hundred-fold than those derived from PEA and tyramine (Table 2). We previously suggested that the proton-abstracting catalytic base (Asp298) also participates in the hydrolysis of TPQ_{psb} by raising the basicity of the water molecule attacking the imine carbon atom (Scheme 1, D′) (*7*). Thus, a longer distance between the carboxyl group of Asp298 and the imine carbon atom of the presumed benzylamine-derived

TPQ_{psb} could be a reason for the greatly decreased rate constant (k_{+3}) in this step; although the water molecule involved in the hydrolysis of TPQ_{psb} has not been identified crystallographically. Finally, the moderately decreased rate constant in the step of $TPQ_{ox} \rightarrow TPQ_{ssb}$ in the reaction with benzylamine (k_{+1}, Table 2) is not interpretable in the absence of the crystal structure of the Michaelis complex.

In conclusion, X-ray crystal structures of AGAO complexed with three different hydrazine derivatives have provided novel structural insights into the substrate specificity of AGAO. Based on the structures of the TPQ/hydrazine adducts, the reactivities of PEA and tyramine as preferred substrates and also of benzylamine as a poor substrate for AGAO have been discussed. Furthermore, an induced-fit movement of substrate (inhibitor)-binding residues has been identified for the first time in CAOs.

Acknowledgements

The X-ray diffraction data were obtained at the beam line BL44XU in SPring-8 with the approval of the Institute for Protein Research, Osaka University.

Funding

This research is supported by Grants-in-Aid for Scientific Research from Japan Society for the Promotion of Science: Young Scientists (B) to T.M. (#11023838) and M.T. (#19750139); and Scientific Research (B) to Y.Y. (#19350084) and T.O. (#18350085).

Conflict of interest

None declared.

References

1. Knowles, P.F. and Dooley, D.M. (1994) Amine oxidases, in *Metal Ions in Biological Systems* (Sigel, H. and Sigel, A., eds.) Vol. 30, pp. 361–403, Marcel Dekker, New York
2. Floris, G. and Mondovi, B. (eds.) (2009) *Copper Amine Oxidases. Structures, Catalytic Mechanisms, and Role in Pathophysiology*, CRC Press, Taylor & Francis Group, Boca Raton, FL
3. Matsuzaki, R., Fukui, T., Sato, H., Ozaki, Y., and Tanizawa, K. (1994) Generation of the topa quinone cofactor in bacterial monoamine oxidase by cupric ion-dependent autooxidation of a specific tyrosyl residue. *FEBS Lett*. **351**, 360–364
4. Cai, D. and Klinman, J.P. (1994) Evidence of a self-catalytic mechanism of 2,4,5-trihydroxyphenylalanine quinone biogenesis in yeast copper amine oxidase. *J. Biol. Chem*. **269**, 32039–32042
5. Choi, Y.H., Matsuzaki, R., Fukui, T., Shimizu, E., Yorifuji, T., Sato, H., Ozaki, Y., and Tanizawa, K. (1995) Copper/topa quinone-containing histamine oxidase from Arthrobacter globiformis. Molecular cloning and sequencing, overproduction of precursor enzyme, and generation of topa quinone cofactor. *J. Biol. Chem*. **270**, 4712–4720
6. Kishishita, S., Okajima, T., Kim, M., Yamaguchi, H., Hirota, S., Suzuki, S., Kuroda, S., Tanizawa, K., and Mure, M. (2003) Role of copper ion in bacterial copper amine oxidase: spectroscopic and crystallographic studies of metal-substituted enzymes. *J. Am. Chem. Soc*. **125**, 1041–1055
7. Chiu, Y.C., Okajima, T., Murakawa, T., Uchida, M., Taki, M., Hirota, S., Kim, M., Yamaguchi, H., Kawano, Y., Kamiya, N., Kuroda, S., Hayashi, H., Yamamoto, Y., and Tanizawa, K. (2006) Kinetic and structural studies on the catalytic role of the aspartic acid residue conserved in copper amine oxidase. *Biochemistry* **45**, 4105–4120
8. Suzuki, S., Okajima, T., Tanizawa, K., and Mure, M. (2009) Cofactors of amine oxidases: Copper ion and its substitution and the 2,4,5-trihydroxylphenylalanine quinone, in *Copper Amine Oxidases. Structures, Catalytic Mechanisms, and Role in Pathophysiology* (Floris, G. and Mondovi, B., eds.), pp. 19–37, CRC Press, Taylor & Francis Group, Boca Raton, FL
9. Taki, M., Murakawa, T., Nakamoto, T., Uchida, M., Hayashi, H., Tanizawa, K., Yamamoto, Y., and Okajima, T. (2008) Further insight into the mechanism of stereoselective proton abstraction by bacterial copper amine oxidase. *Biochemistry* **47**, 7726–7733
10. Shepard, E.M., Okonski, K.M., and Dooley, D.M. (2008) Kinetics and spectroscopic evidence that the Cu(I)-semiquinone intermediate reduces molecular oxygen in the oxidative half-reaction of *Arthrobacter globiformis* amine oxidase. *Biochemistry* **47**, 13907–13920
11. Mure, M. and Klinman, J.P. (1995) Model studies of topaquinone-dependent amine oxidases. 2. Characterization of reaction intermediates and mechanism. *J. Am. Chem. Soc*. **117**, 8707–8718
12. Roh, J.H., Suzuki, H., Azakami, H., Yamashita, M., Murooka, Y., and Kumagai, H. (1994) Purification, characterization, and crystallization of monoamine oxidase from *Escherichia coli* K-12. *Biosci. Biotech. Bbiochem* **58**, 1652–1656
13. Shimizu, E., Ohta, K., Takayama, S., Kitagaki, Y., Tanizawa, K., and Yorifuji, T. (1997) Purification and properties of phenylethylamine oxidase of *Arthrobacter globiformis*. *Biosci. Biotech. Biochem*. **61**, 501–505
14. Cai, D. and Klinman, J.P. (1994) Copper amine oxidase: heterologous expression, purification, and characterization of an active enzyme in *Saccharomyces cerevisiae*. *Biochemistry* **33**, 7647–7653
15. Hevel, J.M., Mills, S.A., and Klinman, J.P. (1999) Mutation of a strictly conserved, active-site residue alters substrate specificity and cofactor biogenesis in a copper amine oxidase. *Biochemistry* **38**, 3683–3693
16. Chang, C.M., Klema, V.J., Johnson, B.J., Mure, M., Klinman, J.P., and Wilmot, C.M. (2010) Kinetic and structural analysis of substrate specificity in two copper amine oxidases from *Hansenula polymorpha*. *Biochemistry* **49**, 2540–2550
17. Agostinelli, E., De Matteis, G., Mondovì, B., and Morpurgo, L. (1998) Reconstitution of Cu^{2+}-depleted bovine serum amine oxidase with Co^{2+}. *Biochem. J*. **330**, 383–387
18. Pietrangeli, P., Federico, R., Mondovì, B., and Morpurgo, L. (2007) Substrate specificity of copper-containing plant amine oxidases. *J. Inorg. Biochem*. **101**, 997–1004
19. Lunelli, M., Di Paolo, M.L., Biadene, M., Calderone, V., Battistutta, R., Scarpa, M., Rigo, A., and Zanotti, G. (2005) Crystal structure of amine oxidase from bovine serum, *J. Mol. Biol*. **346**, 991–1004
20. Duff, A.P., Cohen, A.E., Ellis, P.J., Kuchar, J.A, Langley, D.B., Shepard, E.M., Dooley, D.M., Freeman, H.C., and Guss, J.M. (2003) The crystal structure of *Pichia pastoris* lysyl oxidase. *Biochemistry* **42**, 15148–15157

21. Janes, S.M. and Klinman, J.P. (1991) An investigation of bovine serum amine oxidase active site stoichiometry: evidence for an aminotransferase mechanism involving two carbonyl cofactors per enzyme dimer. *Biochemistry* **30**, 4599–4605
22. Morpurgo, L., Agostinelli, E., Mondovi, B., Avigliano, L., Silvestri, R., Stefancich, G., and Artico, M. (1992) Bovine serum amine oxidase: half-site reactivity with phenylhydrazine, semicarbazide, and aromatic hydrazides. *Biochemistry* **31**, 2615–2621
23. Medda, R., Padiglia, A., Pedersen, J.Z., Rotilio, G., Finazzi Agrò, A., and Floris, G. (1995) The reaction mechanism of copper amine oxidase: detection of intermediates by the use of substrates and inhibitors. *Biochemistry* **34**, 16375–16381
24. Bellelli, A., Morpurgo, L., Mondovì, B., and Agostinelli, E. (2000) The oxidation and reduction reactions of bovine serum amine oxidase. A kinetic study. *Eur. J. Biochem.* **267**, 3264–3269
25. Mure, M. and Klinman, J.P. (1993) Synthesis and spectroscopic characterization of model compounds for the active site cofactor in copper amine oxidases. *J. Am. Chem. Soc.* **115**, 7117–7127
26. Mure, M., Brown, D.E., Saysell, C., Rogers, M.S., Wilmot, C.M., Kurtis, C.R., McPherson, M.J., Phillips, S.E.V., Knowles, P.F., and Dooley, D.M. (2005) Role of the interactions between the active site base and the substrate Schiff base in amine oxidase catalysis. Evidence from structural and spectroscopic studies of the 2-hydrazinopyridine adduct of Escherichia coli amine oxidase. *Biochemistry* **44**, 1568–1582
27. Mure, M., Kurtis, C.R., Brown, D.E., Rogers, M.S., Tambyrajah, W.S., Saysell, C., Wilmot, C.M., Phillips, S.E.V., Knowles, P.F., Dooley, D.M., and McPherson, M.J. (2005) Active site rearrangement of the 2-hydrazinopyridine adduct in *Escherichia coli* amine oxidase to an azo copper(II) chelate form: a key role for tyrosine 369 in controlling the mobility of the TPQ-2HP adduct. *Biochemistry* **44**, 1583–1594
28. Mills, S.A. and Klinman, J.P. (2000) Evidence against reduction of Cu^{2+} to Cu^{+} during dioxygen activation in a copper amine oxidase from yeast. *J. Am. Chem. Soc.* **122**, 9897–9904
29. Leslie, A.G.W. (1992) *Joint CCP4 and EESF-EACMB Newsletter on Protein Crystallography*. SERC Daresbury Laboratory, Warrington, UK
30. Collaborative Computational Project Number 4 (1994) The CCP 4 suite: programs for protein crystallography. *Acta Crystallogr.* **D50**, 760–763
31. Wilce, M.C., Dooley, D.M., Freeman, H.C., Guss, J.M., Matsunami, H., McIntire, W.S., Ruggiero, C.E., Tanizawa, K., and Yamaguchi, H. (1997) Crystal structures of the copper-containing amine oxidase from *Arthrobacter globiformis* in the holo and apo forms: implications for the biogenesis of topaquinone. *Biochemistry* **36**, 16116–16133
32. Brünger, A.T., Adams, P.D., Clore, G.M., DeLano, W.L., Gros, P., Grosse-Kunstleve, R.W., Jiang, J.S., Kuszewski, J., Nilges, M., Pannu, N.S., Read, R.J., Rice, L.M., Simonson, T., and Warren, G.L. (1998) Crystallography & NMR system: a new software suite for macromolecular structure determination. *Acta Crystallogr.* **D54**, 905–921
33. McRee, D.E. (1999) XtalView/Xfit–A versatile program for manipulating atomic coordinates and electron density. *J. Struct. Biol.* **125**, 156–165
34. Kleywegt, G.J. and Jones, T.A. (1997) Model building and refinement practice. *Methods Enzymol.* **277**, 208–230
35. Chen, V.B., Arendall, W.B. III, Headd, J.J., Keedy, D.A., Immormino, R.M., Kapral, G.J., Murray, L.W., Richardson, J.S., and Richardson, D.C. (2010) MolProbity: all-atom structure validation for macromolecular crystallography. *Acta Crystallogr.* **D66**, 12–21
36. Murakawa, T., Okajima, T., Kuroda, S., Nakamoto, T., Taki, M., Yamamoto, Y., Hayashi, H., and Tanizawa, K. (2006) Quantum mechanical hydrogen tunneling in bacterial copper amine oxidase reaction. *Biochem. Biophys. Res. Commun.* **342**, 414–423
37. Hirota, S., Iwamoto, T., Kishishita, S., Okajima, T., Yamauchi, O., and Tanizawa, K. (2001) Spectroscopic observation of intermediates formed during the oxidative half-reaction of copper/topa quinone-containing phenylethylamine oxidase. *Biochemistry* **40**, 15789–15796
38. Frébort, I., Toyama, H., Matsushita, K., and Adachi, O. (1995) Half-site reactivity with *p*-nitrophenylhydrazine and subunit separation of the dimeric copper-containing amine oxidase from *Aspergillus niger*. *Biochem. Mol. Biol. Int.* **36**, 1207–1216
39. Schwartz, B., Green, E.L., Sanders-Loehr, J., and Klinman, J.P. (1998) Relationship between conserved consensus site residues and the productive conformation for the TPQ cofactor in a copper-containing amine oxidase from yeast. *Biochemistry* **37**, 16591–16600
40. Plastino, J., Green, E.L., Sanders-Loehr, J., and Klinman, J.P. (1999) An unexpected role for the active site base in cofactor orientation and flexibility in the copper amine oxidase from *Hansenula polymorpha*. *Biochemistry* **38**, 8204–8216
41. Green, E.L., Nakamura, N., Dooley, D.M., Klinman, J.P., and Sanders-Loehr, J. (2002) Rates of oxygen and hydrogen exchange as indicators of TPQ cofactor orientation in amine oxidases. *Biochemistry* **41**, 687–696
42. Mure, M., Mills, S.A., and Klinman, J.P. (2002) Catalytic mechanism of the topa quinone containing copper amine oxidases. *Biochemistry* **41**, 9269–9278
43. Wilmot, C.M., Murray, J.M., Alton, G., Parsons, M.R., Convery, M.A, Blakeley, V., Corner, A.S., Palcic, M.M., Knowles, P.F., McPherson, M.J., and Phillips, S.E.V. (1997) Catalytic mechanism of the quinoenzyme amine oxidase from *Escherichia coli*: Exploring the reductive half-reaction. *Biochemistry* **36**, 1608–1620
44. Langley, D.B., Trambaiolo, D.M., Duff, A.P., Dooley, D.M., Freeman, H.C., and Guss, J.M. (2008) Complexes of the copper-containing amine oxidase from *Arthrobacter globiformis* with the inhibitors benzylhydrazine and tranylcypromine. *Acta Crystallogr* **F64**, 577–583
45. Matsuzaki, R. and Tanizawa, K. (1998) Exploring a channel to the active site of copper/topaquinone-containing phenylethylamine oxidase by chemical modification and site-specific mutagenesis. *Biochemistry* **37**, 13947–13957